Small-Animal Dark-Field Radiography for Pulmonary Emphysema Evaluation

Andre Yaroshenko*¹, Felix G. Meinel², Katharina Hellbach², Martin Bech^{1,3}, Astrid Velroyen¹, Mark Müller¹, Fabian Bamberg², Konstantin Nikolaou², Maximilian F. Reiser², Ali Ö. Yildirim⁴, Oliver Eickelberg⁴, Franz Pfeiffer¹

 Lehrstuhl für Biomedizinische Physik, Physik-Department & Institut für Medizintechnik, Technische Universität München, 85748 Garching, Germany
Institute for Clinical Radiology, Ludwig-Maximilians-University Hospital Munich, Marchioninistr. 15, 81377 München, Germany.

³ Medical Radiation Physics, Lund University, 22185 Lund, Sweden.

ABSTRACT

Chronic obstructive pulmonary disease (COPD) is one of the leading causes of morbidity and mortality worldwide and emphysema is one of its main components. The disorder is characterized by irreversible destruction of the alveolar walls and enlargement of distal airspaces. Despite the severe changes in the lung tissue morphology, conventional chest radiographs have only a limited sensitivity for the detection of mild to moderate emphysema. X-ray dark-field is an imaging modality that can significantly increase the visibility of lung tissue on radiographic images. The dark-field signal is generated by coherent, small-angle scattering of x-rays on the air-tissue interfaces in the lung. Therefore, morphological changes in the lung can be clearly visualized on dark-field images. This is demonstrated by a preclinical study with a small-animal emphysema model. To generate a murine model of pulmonary emphysema, a female C57BL/6N mouse was treated with a single orotracheal application of porcine pancreatic elastase (80 U/kg body weight) dissolved in phosphate-buffered saline (PBS). Control mouse received PBS. The mice were imaged using a small-animal dark-field scanner. While conventional x-ray transmission radiography images revealed only subtle indirect signs of the pulmonary disorder, the difference between healthy and emphysematous lungs could be clearly directly visualized on the dark-field images. The dose applied to the animals is compatible with longitudinal studies. The imaging results correlate well with histology. The results of this study reveal the high potential of dark-field radiography for clinical lung imaging.

Keywords: x-ray phase-contrast imaging, x-ray dark-field, grating interferometer, pulmonary emphysema, COPD.

1. INTRODUCTION

Pulmonary emphysema is one of the main components of the Chronic Obstructive Pulmonary Disease (COPD), which is one of the leading causes of mortality and morbidity worldwide^{1,2}. One of the causes for pulmonary emphysema is smoking. The pulmonary disorder is characterized by severe changes in the lung tissue morphology, like irreversible destruction of the alveolar walls and enlargement of distal airspaces.

Conventional, absorption-based x-ray imaging has only a limited sensitivity for mild to moderate emphysema³. Therefore, it is very challenging to diagnose pulmonary emphysema based on conventional x-ray chest radiographs alone. Therefore, pulmonary emphysema is usually diagnosed using conventional x-ray CT⁴. However, the high patient radiation dose limits the application of CT for screenings and frequent follow-up examinations. Furthermore, only high resolution CT (HRCT) is suitable for detection of emphysema at early stages of the disorder. And yet, assessing the regional distribution of pulmonary emphysema is crucial for clinical decision-making concerning e.g. lung volume reduction surgery. It has been suggested in some studies that MRI imaging can be used to complement CT for pulmonary imaging³. However, MRI is not an established routine for COPD imaging due to long image acquisition time, high costs

Medical Imaging 2014: Physics of Medical Imaging, edited by Bruce R. Whiting, Christoph Hoeschen, Despina Kontos, Proc. of SPIE Vol. 9033, 90331M ⋅ © 2014 SPIE ⋅ CCC code: 1605-7422/14/\$18 ⋅ doi: 10.1117/12.2042995

Proc. of SPIE Vol. 9033 90331M-1

⁴ Comprehensive Pneumology Center, Institute of Lung Biology and Disease, Helmholtz Zentrum Munich, Ingolstädter Landstr. 1, 85764 Neuherberg, Germany.

and low availability. Furthermore, MRI is more prone to breathing artifacts than CT. Thus, the only established technique to monitor the disease progression, as of now, is histopathology, which requires invasive biopsy.

X-ray phase-contrast is an imaging technique that can yield a significantly higher contrast and complementary information in the soft tissue. Different approaches to acquire the phase information for x-ray imaging have been studied at large-scale synchrotron facilities starting from the first experiments carried out by Bonse and Hart around 1965^{5,6,7}. Several further techniques have been developed since then. Among the most known approaches are the propagation based approach^{8,9,10}, the analyzer-based approach^{11,12} and the grating-based approach^{7,13,14}. However, only recently a method has been reported how the grating-based approach can be adapted to acquire phase information using a compact, polychromatic laboratory source^{14,15}.

To acquire differential phase-contrast and dark-field using a compact, polychromatic laboratory source, a three-grating Talbot-Lau interferometer is introduced into the beam. The first (absorption) grating is placed right downstream of the source. This grating, referred to as the source grating, introduces sufficient lateral coherence into the beam. A second (phase) grating is then placed in the beam. This grating introduces a well-defined interference pattern (Lohmann image) at a known distance downstream of the grating. Typically gratings with binary $\pi/2^{16}$ or $\pi^{17,18}$ phase-shifting structures are used. The ratio of the grating opening to the grating structure is commonly 1:1. The interference pattern is typically too small to be directly resolved by the detector. Therefore, a third (absorption) grating is placed just in front of the detector. This grating is referred to as the analyzer grating. A number of images are acquired moving the analyzer grating in a number of steps over one grating period. In this way a so-called intensity stepping curve¹⁹ is acquired for each detector pixel. The distance between the phase and the analyzer grating is defined by the phase grating parameters. For the $\pi/2$ grating, the shortest distance for the Lohmann image is given by $Z_t/4^{20}$, where Z_t is the full Talbot distance: $Z_t=2p^2/\lambda$, where p is the grating period and λ the wavelength. For a phase grating with π phase shifting structures, the shortest distance is given by $Z_t/16^{20}$. However, in this case the Lohmann image has twice the frequency of the phase grating. The absorption gratings are produced with x-ray lithography and have pitches in the range of 2-10 μ m with a height of the structures of around 150 μ m. Due to production limitations, it is not always possible to produce an absorption grating with half the period of the phase grating.

Using Talbot-Lau grating interferometer, the conventional absorption, the differential phase-contrast and the dark-field images are acquired simultaneously. The three signals are obtained from the stepping curve, which is acquired once with and once without the sample in the beam. The mean value of the stepping curve acquired with the sample divided by the mean value of the corresponding stepping curve without the sample represents the transmission signal. The phase shift between the two stepping curves gives the differential phase-contrast. Finally, the ratio of the amplitudes of the stepping curves with and without the sample, normalized by the transmission signal yields the dark-field signal. The dark-field signal originates from the coherent small-angle scattering in the sample. Typically, the structures that can be seen in the dark field have sub-pixel dimensions.

Recently, it has been reported that dark-field imaging can significantly increase lung tissue visibility on projection images, acquired with a compact, polychromatic laboratory source²¹. X-rays are scattered on the alveoli in the lung and give a strong dark-field signal. Morphological changes in the lung tissue lead to visible changes in the signal strength. Thus, first proof-of-principle experiments with excised *ex vivo* murine samples demonstrated that the morphological changes due to pulmonary emphysema can be visualized directly in the dark-field^{22,23,24,25}. Furthermore, it was shown that combination of conventional transmission and dark-field signal leads to an increased diagnostic value for pulmonary emphysema, compared to the diagnostic value of each of the two imaging modalities alone.

It has been broadly questioned whether the improved diagnostic value for pulmonary disorders, obtained in the dark-field for excised murine lungs can be transferred to *in vivo* imaging. It can be argued that the overlaying structures like fur and bones can potentially destroy the signal so far, that no additional value can be obtained from the dark-field image. The purpose of the present study was to demonstrate that the dark-field radiography has improved diagnostic value for detection of pulmonary emphysema also for *ex vivo* animals with lungs *in situ*.

2. MATERIALS AND METHODS

2.1 Prototype Scanner

The imaging experiments were carried out with a prototype small-animal x-ray phase-contrast and dark-field CT scanner ¹⁶ (Figure 1 (A)). The scanner consists of a rotating gantry built into a housing suitable for preclinical small-animal imaging. A schematic sketch of the gantry is shown in Figure 1 (B).

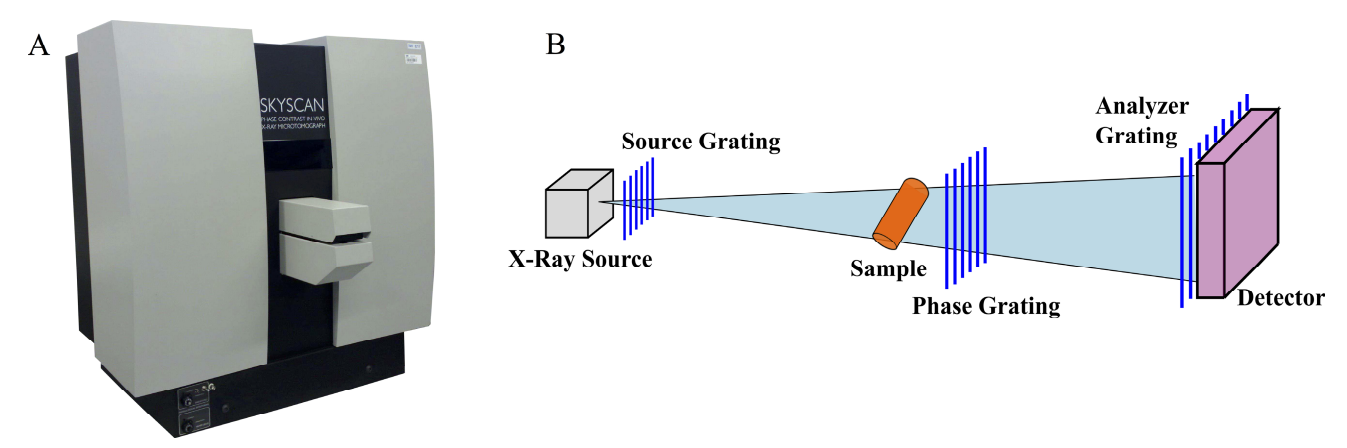


Figure 1: (A) Photograph of the prototype small-animal CT scanner. The scanner dimensions are approximately 1 x 0.95 x 0.8 m³. (B) Sketch of the setup installed on the rotating gantry in the scanner.

The setup installed on the rotating gantry consists of an x-ray source, a specimen opening, a detector and a three-grating Talbot-Lau interferometer. The sample bed is situated immediately in front of the phase grating. The x-ray source is a fixed anode tungsten-target tube (RTW, MCBM 65B-50 W, approximately 50 μ m focal spot size in diameter). The detector is a flat-panel Hamamatsu, C9312SK-06, GOS scintillator, with 50 μ m pixel size. The active area is 124.8 \times 115.2 mm². The sample field of view is 3.5 \times 2.5 cm². The source grating (period 10 μ m, gold height 35 μ m) is 300 mm away from the phase grating (period 3.24 μ m, nickel height 4.0 μ m, phase shift π /2). And the analyser grating (period 4.8 μ m, gold height 45 μ m) is positioned 145 mm behind the phase grating. The x-ray emission point of the tube lies 3 cm away from the source grating. The analyser grating is positioned in immediate contact with the detector. The interferometer is operated at the first fractional Talbot distance.

2.2 Murine Pulmonary Emphysema Protocol

Animal experiments were performed with permission of the responsible Institutional Animal Care and Use Committee. Experiments were performed according to national (GV-SOLAS) and international (FELASA) animal welfare guidelines. Eight week old pathogen-free female C57BL/6N (Charles River Laboratories, Sulzfeld, Germany) mice were used in this study. For the induction of pulmonary emphysema the mouse received orotracheally a solution of pancreatic elastase in a sterile phosphate-buffered saline (80 U/kg body weight). Control mouse received 80 μ l of only sterile phosphate-buffered saline. Mice were sacrificed 21 days after elastase application and imaged shortly afterwards.

2.3 Imaging Protocol

A healthy mouse was imaged *in vivo* with the source voltage set at 30 kVp and the total source power was 15 W. The images were acquired with 10 steps of the source grating over one grating period with an exposure time of 10 seconds per step. During image acquisition the animal temperature and the breathing rate were being monitored continuously, while the mouse was breathing freely.

Two freshly dead mice were imaged at 35 kVp source voltage and 18 W source power. 10 phase steps were acquired with an exposure time of 5 seconds per step.

Proc. of SPIE Vol. 9033 90331M-3

2.4 Histology.

The lungs were excised, filled with air, tied at the trachea and placed in paraformaldehyde for transportation. Subsequently, paraformaldehyde was washed off and the lungs were decalcified in a 10 % EDTA solution for 5 days. The samples were dehydrated and embedded in paraffin. Multiple 10 µm thin slices were prepared in the coronal plane. The slices were deparaffinized, hydrated and stained using Mayer's hematoxylin and eosin (H&E) staining routine protocol. Finally, the sections were scanned using a microscope.

2.5 Dose Estimation

To estimate the animal dose a patient skin dosimeter (Unfors PSD, Unfors Instruments AB, Billdal, Sweden) was placed in the center of a polymer cylinder with a 3 cm diameter. The polymer cylinder is a good approximation for a mouse phantom. With the cylinder placed in the beam, the dose was estimated for 10 minutes to obtain better statistics. The mouse scan dose was subsequently calculated from the measured dose.

3. RESULTS

Imaging results for a healthy mouse *in vivo* can be seen in Figure 2. Relative to the soft tissue, bones have a high absorption coefficient. Hence, they are clearly visible on the conventional x-ray absorption-based radiograph (Figure 2 (A)). On the contrary, different soft tissue organs have only a slightly varying absorption coefficient. Therefore, conventional absorption-based x-ray imaging does not yield sufficient contrast to discriminate between different organs.

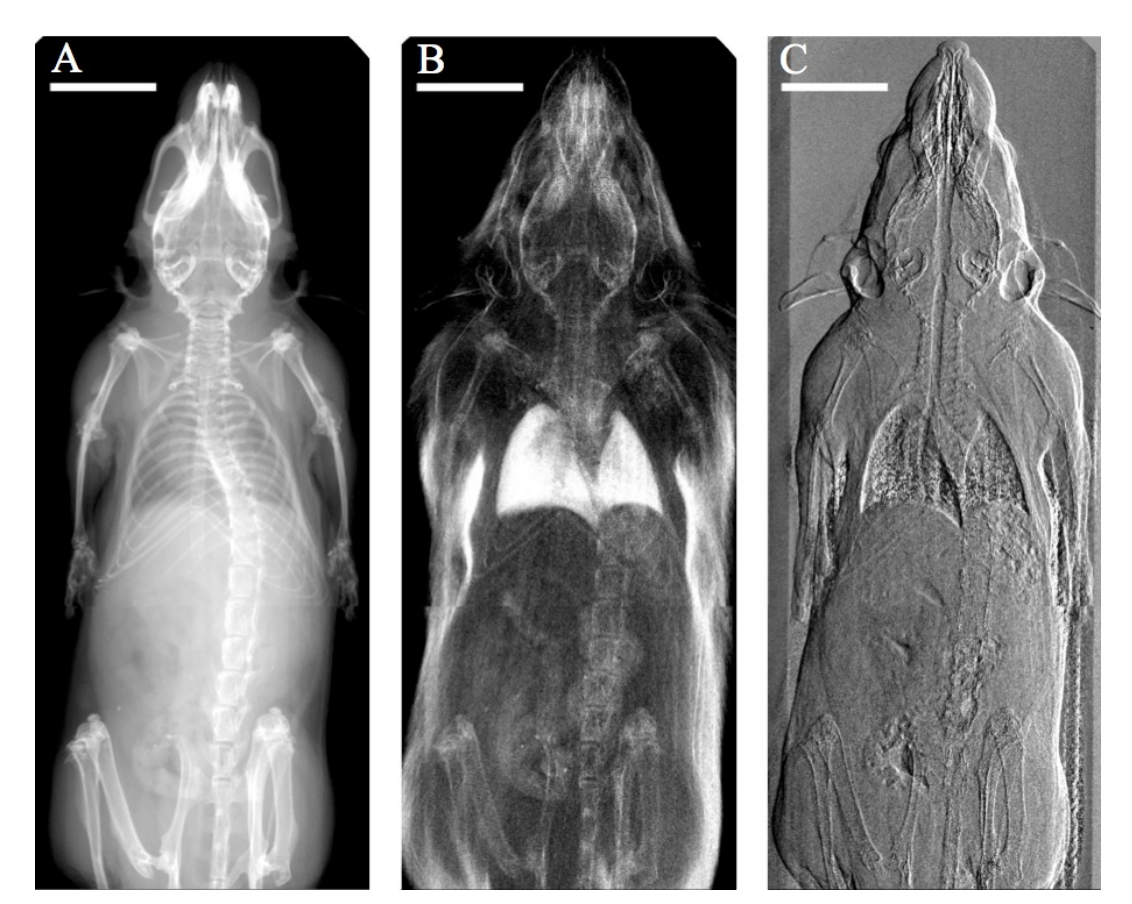


Figure 2: (A) Conventional x-ray transmission (B) dark-field and (C) differential phase-contrast image of a mouse acquired *in-vivo*. White scale bars correspond to 1 cm.

X-ray are scattered on the interfaces between air and tissue in the lung (alveoli). This yields a strong dark-field signal, as can be seen in Figure 2 (B). The lungs tissue is clearly visible, although it is overlaid with fur, bones and further

structures. Furthermore, although the image was acquired with the animal breathing freely during image acquisition, the lung does not appear to be excessively blurred. The lung tissue visibility is significantly better than in the transmission image. The x-rays are also scattered significantly on the fur of the animal, which is also clearly visible in the dark-field. The bones of the animal are also visible in the dark-field. However, this is mainly due to the beam hardening effect. High absorption, leads to a signal also in the dark-field. However, the nature of this signal is not x-ray scattering but high absorption.

Finally, the differential phase-contrast image reveals all the edges with an enhanced contrast. It is interesting to notice that the trachea of the mouse appears very distinctly on the projection image. The trachea is visible neither on the dark-field nor on the absorption image. Therefore, differential phase-contrast could be a suitable imaging modality for trachea disorders.

Images presented in Figure 2 are stitched together, as the field of view of the scanner is not large enough to fit the whole animal into the field of view. The total animal dose for the acquisition is estimated with 3.9 mGy.

Figure 3 shows all three imaging modalities for an *ex vivo* healthy mouse and a mouse with pulmonary emphysema. The corresponding imaging modalities for the two animals are windowed in the same way to facilitate comparison. The total animal dose for the acquisition is 5,4 mGy.

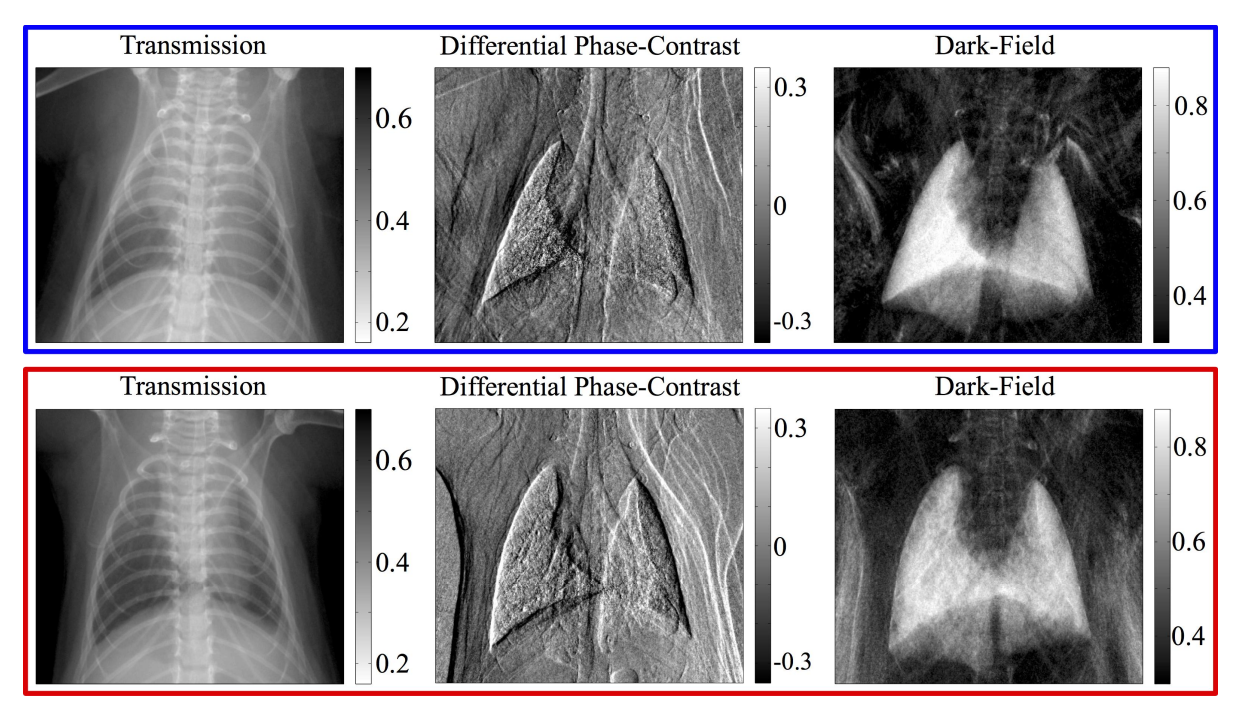
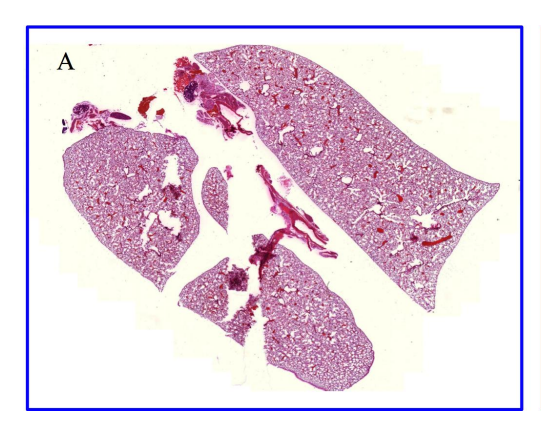


Figure 3: Top (blue): Transmission, differential phase-contrast and dark-field radiographs of an *ex vivo* control mouse. Bottom (red): corresponding images of an *ex vivo* mouse with pulmonary emphysema. Image acquisition parameters: 10 phase steps of the source grating with an exposure time of 5 seconds per step, no binning of the detector.

While it is difficult to detect the pulmonary disorder, from the absorption image alone, the difference between healthy and emphysematous lung can be clearly seen on the dark-field images. Destruction of the alveolar network in the emphysema lung leads to less scattering and thus a weaker dark-field signal. While the outline of the healthy lung on the dark-field image is clearly visible, the outline of the emphysematous lung appears blurry. The pulmonary disorder is especially clearly visible in the peripheral area.



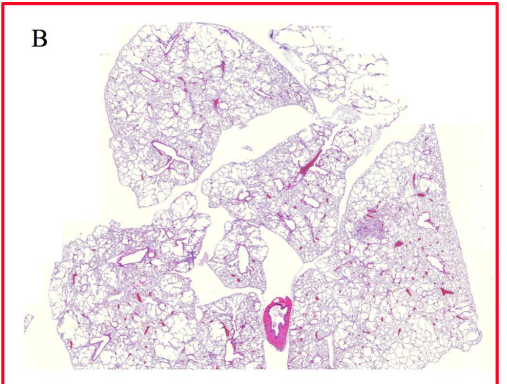


Figure 4: (A) Histology section of the control murine lung. A dense alveolar network is clearly visible. (B) Histology section of the murine lung with pulmonary emphysema. Distal airspaces are clearly enlarged, confirming introduction of pulmonary emphysema.

Introduction of the pulmonary disorder was confirmed using histology. Figure 4 shows histological sections of the two lungs. The images were acquired using the same magnification. The histology section of the control lung shows a dense alveolar network. The lung from the emphysema mouse shows, on the contrary, enlarged distal airspaces and confirms thus, successful introduction of pulmonary emphysema.

4. DISCUSSION

The presented results have shown that pulmonary emphysema can be directly visualized in the dark-field also for *ex vivo* animals with lungs *in situ*. The overlaying structures do not distort the signal excessively. Even if the dose of 5,4 mGy is low enough for repetitive studies, it is interesting to analyze if the necessary dose can be further reduced, by acquiring less phase steps and using larger pixel sizes.

In order to analyze this, the images presented in Figure 3 were reprocessed using a 4x4 detector binning and using only every second phase step (in total 5 steps). Thus, obtained images are shown in Figure 5.

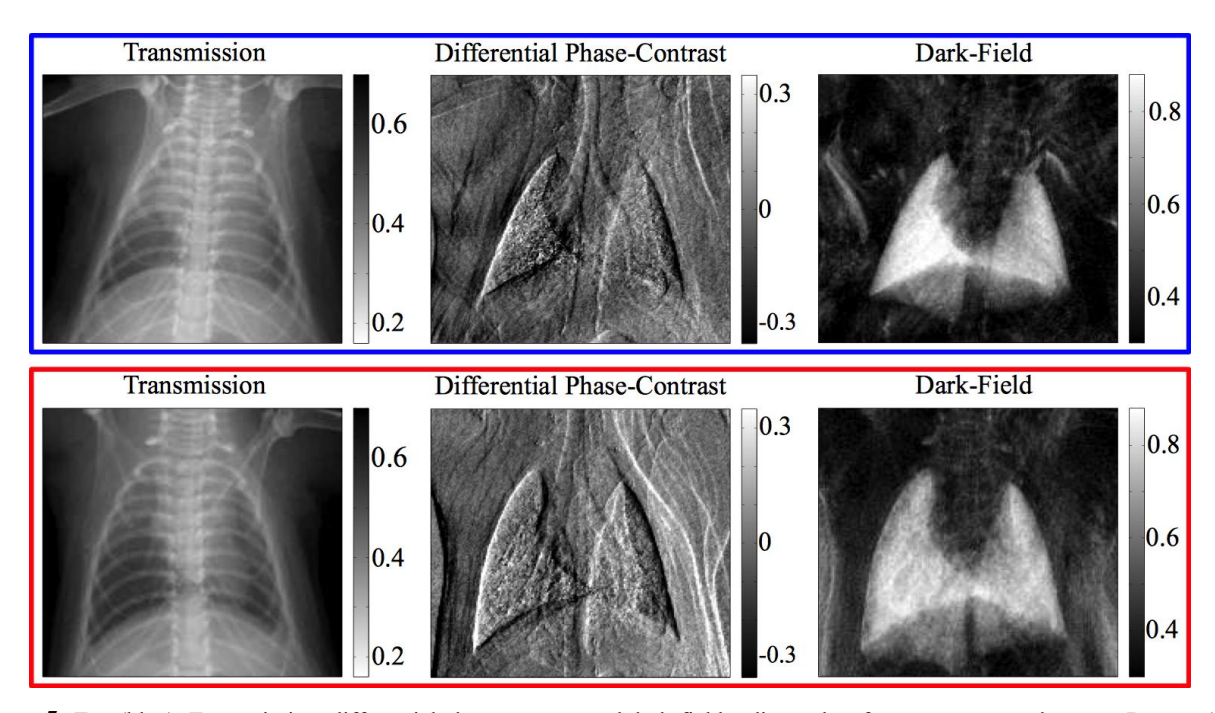


Figure 5: Top (blue): Transmission, differential phase-contrast and dark-field radiographs of an *ex vivo* control mouse. Bottom (red): corresponding images of an *ex vivo* mouse with pulmonary emphysema. The images were processed using only 5 phase steps of the source grating with an exposure time of 5 seconds per step. A 4 x 4 binning was applied to the detector.

Even if the resolution of the images is reduced by a factor of 4, the difference between healthy and emphysematous lung can be still clearly seen in the dark-field. This is a very interesting result. First, it means that the necessary dose can be reduced by a factor of 32, resulting in a dose of 0,17 mGy. Second, this means that the morphological changes in the lung can be also observed with a detector with a pixel size of 200 x 200 μ m². This resolution is compatible with pixel sizes used for clinical imaging devices.

The presented study has also some limitations. The study was performed on *ex vivo* animals. The dark-field signal strongly depends on the amount of air/tissue interfaces and it is not trivial to achieve exactly the same amount of air in the lung of a healthy and an emphysematous mouse. Therefore, this can distort the result. Future studies should focus on performing experiments on living animals. However, for this case breathing artifacts have to be taken into account. Furthermore, this study was performed only on one mouse from each group. Future studies should be based on more statistics. Moreover, the animal with pulmonary emphysema was imaged at a relatively late stage of the disorder. It should be analyzed if the results are comparable for animals with earlier stages of pulmonary emphysema.

In conclusion, this is a proof-of-principle study that reveals the high potential of dark-field imaging for pulmonary emphysema in murine models.

Acknowledgement

We acknowledge the financial support through the DFG Cluster of Excellence Munich-Centre for Advanced Photonics (MAP), the DFG Gottfried Wilhelm Leibniz program and the European Research Council (ERC, FP7, StG 240142). A.Y., A.V., acknowledge the TUM Graduate School for the support of their studies.

5. REFERENCES

- [1] Zvezdin B., Milutinov S., Kojicic M., et al. "A postmortem analysis of major causes of early death in patients hospitalized with COPD exacerbation" Chest 136, 376-380 (2009).
- [2] Celli B.R., MacNee W.R., "Standards for the diagnosis and treatment of patients with COPD: a summary of the ats/ers position paper" Eur Respir J 23, 932-946 (2004).
- [3] Washko GR., "Diagnostic imaging in COPD" Semin Respir Crit Care Med 31, 276-285 (2010).
- [4] Kauczor H.U., Heussel C.P., Herth F.JF., "Longitudinal quantitative low-dose CT in COPD: ready for use?" The Lancet Respiratory Medicine 1(2), 95-96 (2013).
- [5] Bonse U., Hart, M. "An x-ray interferometer with long separated interfering beam paths" Appl. Phys. Lett. 6, 155–156 (1965).
- [6] Beckmann F., Bonse, U., Busch, F. and Günnewig, O., "X-ray micro- tomography (μCT) using phase contrast for the investigation of organic matter" Journal of Computer Assisted Tomography 21(4), 539–553 (1997).
- [7] Momose A., Kawamoto S., Koyama I., Hamaishi Y., Takai K. and Suzuki, Y., "Demonstration of x-ray Talbot interferometry" Jpn. J. Appl. Phys 42, 866–868 (2003).
- [8] Snigirev A., Snigireva I., Kohn, V., Kuznetsov S. and Schelokov I., "On the possibilities of x-ray phase contrast microimaging by coherent high-energy synchrotron radiation" Rev. Sci. Instrum 66(12), 5486–5492 (1995).
- [9] Wilkins S.W., Gureyev T.E., Gao D., Pogany A. and Stevenson, A.W., "Phase-contrast imaging using polychromatic hard x-rays" Nature 384, 335–337 (1996).
- [10] Cloetens P., Ludwig W., Baruchel J., Dyck D.V., Landuyt J. V., Guigay, J.P. and Schlenker M., "Holotomography: Quantitative phase tomography with micrometer resolution using hard synchrotron radiation x rays" Appl. Phys. Lett 75(19), 2912–2914 (1999).
- [11] Ingal V. and Beliaevskaya E., "X-ray plane-wave topography observation of the phase contrast from a non-crystalline object" J. Phys. D Appl. Phys 28, 2314–2317 (1995).
- [12] Davis T.J., Gao D., Gureyev T.E., Stevenson A.W. and Wilkins S.W., "Phase-contrast imaging of weakly absorbing materials using hard x-rays" Nature 373, 595–598 (1995).
- [13] David C., Nöhammer B., Solak H.H. and Ziegler E., "Differential x-ray phase contrast imaging using a shearing interferometer" Appl. Phys. Lett 81(17), 3287–3289 (2002).
- [14] Pfeiffer F., Weitkamp T., Bunk O. and David C., "Phase retrieval and differential phase-contrast imaging with low-brilliance x-ray sources" Nat. Phys 2, 258–261 (2006).

- [15] Pfeiffer F., Bech M., Bunk O., Kraft P., Eikenberry E.F., Brönnimann C., Grünzweig C. and David C., "Hard-x-ray dark-field imaging using a grating interferometer" Nat. Mater 7, 134–137 (2008).
- [16] Tapfer A., Bech M., Velroyen A., Meiser J., Mohr J., Walter J., Schulz J., Pauwels B., Bruyndonckx P., Liu X., Sasov A., and Pfeiffer F., "Experimental results from a preclinical X-ray phase-contrast CT scanner," Proc. Natl. Acad. Sci. U. S. A. 109, 15691–15696 (2012).
- [17] Thüring T., Guggenberger R., Alkadhi H., Hodler J., VichM., Wang Z., David C., and Stampanoni M., "Human hand radiography using X-ray differential phase contrast combined with dark-field imaging," Skeletal Radiol. 42, 827–835 (2013).
- [18] Chen G.H., Bevins N., Zambelli J. and Qi Z., "Small-angle scattering computed tomography (SAS-CT) using a Talbot-Lau interferometer and a rotating anode X-ray tube: theory and experiments," Opt. Express 18, 12960–12970 (2010).
- [19] Weitkamp T., Diaz A., David C., Pfeiffer F., Stampanoni M., Cloetens P., and Ziegler E., "X-ray phase imaging with a grating interferometer," Opt. Express 13, 6296–6304 (2005).
- [20] Suleski T.J., "Generation of Lohmann images from binary-phase Talbot array illuminators," Appl. Opt. **36**, 4686–4691 (1997).
- [21] Bech M., Tapfer A., Velroyen A., Yaroshenko A., Pauwels B., Hostens J., Bruyndonckx P., Sasov A. and Pfeiffer F., "In-vivo dark-field and phase-contrast x-ray imaging" Nat. Scientific Reports, 10.1038/srep03209 (2013).
- [22] Schleede S., Meinel F.G., Bech M., et al. "Emphysema diagnosis using X-ray dark-field at a laser driven compact synchrotron light source" Proc. Natl. Acad. Sci. U. S. A. 109(44), 17880-17885 (2012)
- [23] Yaroshenko A., Meinel F.G., Bech M., et al. "Pulmonary Emphysema Diagnosis with a Preclinical Small-Animal X-ray Dark-Field Scatter-Contrast Scanner" Radiology 269, 427-433 (2013).
- [24] Meinel F.G., Schwab F., Schleede S., et al. "Diagnosing and Mapping Pulmonary Emphysema on X-Ray Projection Images: Incremental Value of Grating-Based X-Ray Dark-Field Imagin" Plos One, 10.1371/journal.pone.0059526 (2013)
- [25] Schwab F., Schleede S., Hahn D., et al. "Comparison of Contrast-to-Noise Ratios of Transmission and Dark-Field Signal in Grating-Based x-ray Imaging for Healthy Murine Lung Tissue" Zeitschrift für Medizinische Physik, 10.1016/j.zemedi.2012.11.003 (2012).